Materials Advances

PAPER

Check for updates

Dispersion engineering of cellulose nanofibres in polyols: for controlled microstructure of high-performance polyurethane foam†

Hima Haridevan, [ID] [ab] David A. C. Evans, [ID] [b] Darren J. Martin [ID] [a] and Pratheep K. Annamalai [ID] *[bcde]

Cellulose nanofibres (CNF) with hydroxyl functional groups are among the most attractive types of functional additive candidates being explored to improve the mechanical and thermal insulation performance of rigid polyurethane foams (RPUF). However, in practice, the poor dispersion of CNF in polyols has hindered the potential enhancements to RPUF using this approach. In this study, CNF/polyol dispersions with a good distribution of CNF in polyol at loadings from 0.03% to 1.12% w/w were used to prepare the CNF/RPUF nanocomposites (CNF/RPUF) containing 0.01% to 0.40% w/w CNF loading. This series of true RPUF nanocomposites represents a better platform to investigate the effect of the CNF on the microstructure, thermal and mechanical properties of RPUF. A CNF/RPUF nanocomposite (0.01% w/w CNF in RPUF) prepared from a dispersion of 0.03% w/w CNF in polyol afforded a 20% reduction in thermal conductivity and a 25% and 56% improvement, respectively, in specific compressive strength and specific modulus. This scale of thermal insulation and mechanical performance improvement for low-density (39 kg m^{-3}) CNF/RPUF systems has not previously been reported.

1. Introduction

Rigid polyurethane foam (RPUF) is the most widely explored material for improved thermal insulation performance given that buildings consume 30% of the produced global energy. They are excellent materials due to their versatile features such as low thermal conductivity, high compressive strength-to-weight ratio, and long-term stability at a low-density regime.

The improvement in thermal insulation performance of RPUF is significantly studied by varying high functionality polyols, surfactants, and micro-/nano-scale functional particulate additives.[1–4] The effectiveness of the particulate additives may be dependent on the method of incorporation,[5,6] quality of dispersion,[4,7–10] host polymer compatibility[9–11] and loading

level[5,12–14] in the RPUF precursors. For example, at an optimal loading, the homogenous distribution of an additive in the polyol media may offer optimal nucleation during foaming, resulting in good microstructure and enhanced performance, whereas the poor distribution (due to less compatible system or inefficient mixing) may lead to re-agglomeration, which in turn may result in damaged microstructure. Above the optimum loading (regardless of quality of dispersion), the microstructural and physical properties[8,15,16] could be adversely affected due to the increase in viscosity of the dispersion, limiting effective mixing with the isocyanates.[4,17] Therefore, achieving a high-quality dispersion of particles at an optimum loading level and maintaining the processibility of the dispersion during foaming are key factors for controlling the microstructure and the thermomechanical properties of the resultant RPUF.[8,9,18,19]

Cellulose nanofibre (CNF) is one such additive material that can be directly incorporated as a filler in RPUF, which also has the potential to interact with the polyol and isocyanate media to obtain RPUF with increased cross-linking strength.[20–23] These nanofibres are flexible and self-interacting (coiling/collapsing, entangling, branched fibrils, bundles) compared to other nanoscale rigid and dimensionally stable nucleating additives (cellulose nanocrystal (CNC),[5,20,24–26] carbon nanotubes,[27] nanoclay,[2,28,29] or graphene oxide[30]).

CNF is typically produced as a wet-dispersion, and this complicates its suitability as a sustainable additive. Typically,

a School of Chemical Engineering, The University of Queensland, Brisbane, 4072, Queensland, Australia

b Australian Institute for Bioengineering and Nanotechnology, The University of Queensland, Brisbane, 4072, Queensland, Australia. E-mail: p.annamalai@uq.edu.au, Pratheep.annamalai@unisq.edu.au

c School of Agriculture and Food Sustainability, The University of Queensland, Brisbane, 4072, Queensland, Australia

d Centre of Future Materials, University of Southern Queensland, Toowoomba, 4350, Queensland, Australia

e School of Agriculture and Environmental Sciences, University of Southern Queensland, Toowoomba, 4350, Queensland, Australia

† Electronic supplementary information (ESI) available. See DOI: https://doi.org/10.1039/d3ma00865g

it has been incorporated in RPUF by redispersion of dehydrated (freeze-dried or spray-dried) powder into polyol by mechanical mixing,[18,19,21] sonication,[5,8] or solvent-assisted dispersion.[9,11] Unfortunately, once dried, CNF additives are not easily dispersible in the polyol media resulting in the agglomerated fibre bundles in polyols, which in turn results in inconsistent/insignificant microstructural variations that affect the physical properties of the RPUF. Hence, ideally, a better CNF/polyol dispersion could be achieved through the incorporation of *never dried* CNF in the polyol matrix.

Previous studies suggest that better dispersion of *never dried* CNF in the polyol could be achieved through a combination of solvent-assisted dispersion with mechanical mixing.[9] However, given that the addition and removal of organic solvents may not be a sustainable solution in terms of scalability and cost-effectiveness,[31] the direct incorporation of CNF/water dispersions followed by the removal of water appears to be a reasonable solution for achieving enhanced dispersion of nanocellulose in the RPUF.

Recently, Haridevan *et al.*[6] reported a methodology for retaining good distribution of CNF in polyols through water-assisted dispersion and scalable vacuum drying of CNF/polyol/water dispersions. These dispersions have resulted in a broad range of viscosity and flow behaviour depending on the CNF loading in the polyol. Herein, we hypothesise that a broad range of rheological properties of these CNF/polyol dispersions pertaining to dispersion methodology and loading level can be adopted for controlling microstructure and consequentially tailoring the physical properties of the RPUF.

To investigate further, CNF/polyol dispersions prepared by water-assisted dispersion, at levels of 0.028 to 1.12% w/w in polyol (reported in Haridevan *et al.*[6]), were used to prepare CNF/RPUF nanocomposites (CNF/RPUF) with resultant loading levels of 0.01 to 0.4% w/w. Given that, it is challenging to directly monitor the influence of rheological properties of the CNF/polyol dispersions on the foaming process, the evaluation of curing kinetics of CNF/polyurethane resins (RPUF formulation *without blowing agent* at an NCO index of 37) using rheological analysis was also attempted to serve as a link between the complex systems of CNF/polyol dispersions and CNF/RPUF. The changes in density, microstructure, compressive mechanical properties, and thermal insulation performance of the RPUF were carefully monitored as the influence of CNF.

The flexibility and the self-interacting nature of CNF (which influenced the rheological behaviour of polyol dispersions[6]) were observed to distinctly influence the microstructural characteristics of RPUF at each loading level. Consequently, CNF/RPUF with a 0.01% w/w CNF loading in RPUF afforded a 20% reduction in thermal conductivity and a 25% and 56% improvement, respectively, in specific compressive strength and modulus perpendicular to foam rise compared to the control RPUF (V0F). At low loading levels, polyols with high degree of dispersion and distribution of CNF were observed to produce low-density foams with significantly enhanced thermal insulation performance. In contrast, the polyol dispersions with higher

CNF loading levels which caused increase in viscosity (due to CNF–CNF interactions) were observed to produce high-density RPUF with (statistically) insignificant improvement in thermal insulation performance. Thus, by successfully demonstrating the correlation of dispersion and distribution of CNF with microstructural, mechanical, and thermal insulation performance of the RPUF, this study shows that the incorporation method for retaining good dispersion of nanoparticulate additive in polyol and the rheological properties of the polyol media are the key determining factors for microstructure and properties of the RPUF.

2. Materials and methods

2.1. Materials

The CNF/polyol dispersions are prepared using a sucrose/glycerol-initiated polyether polyol (Voranol™ 446) and CNF derived from alkali-treated spinifex grass (*Triodia pungens*) pulp as described in Haridevan *et al.*[6] Tegostab® B 8460 from Evonik and dimethylcyclohexamine (DMCHA) from Sigma-Aldrich were utilised as the surfactant and catalyst. HFCM1, a proprietary blend of HFC245a and HFC365mfc from Applied Polymers, was used as the physical blowing agent, while water was used as the chemical blowing agent. The polymeric isocyanate (pMDI) (PAPI 27 of the Dow Chemical Company) with NCO content 31.5% was used as obtained from the Applied Polymers. The mould release agent ERALEASE LP57 was obtained from Era Polymers.

2.2. Preparation of CNF/RPUF nanocomposites

A typical formulation for a basic RPUF, initially proposed by the Dow Chemical Company but slightly modified in our laboratory to accommodate the preparation of foam with polyol and a different blowing agent, is used as the control formulation (V0F) (Table 1). The control RPUF samples V0F and V0SF were prepared using neat polyol (Voranol ™ 446, V0) as-received, and that subjected to high shear mixing treatment (V0S), respectively. This was done to completely replicate the processing history of nanocomposites in the control RPUF sample without the CNF.

The CNF/polyol dispersions with low loadings 0.028% w/w to 0.28% w/w, were used to prepare low-density (<50 kg m^{-3}) CNF/RPUF nanocomposite samples with final CNF loadings of 0.01% w/w to 0.1% w/w (namely VCF0.028, VCF0.07, VCF0.14, VCF0.28), according to the formulations in Table 1. Whereas CNF/polyol dispersions with relatively higher loadings 0.56% w/w to 1.12% w/w in polyol (with high viscosity as determined by rheological measurements) were used to prepare high-density CNF/RPUF with 0.2% w/w to 0.4% w/w CNF loading (VCF0.56, VCF0.84, VCF1.12) respectively, according to the formulations in Table S1 in ESI.† An additional control RPUF (V0F-control 2) was prepared using the same formulation of V0F at a higher-density (63 kg m^{-3}) by *over-packing* the mould with extra mass.

For the polyol blends (Part B), all materials, except the blowing agent, were pre-blended using an overhead stirrer

Table 1 Formulation, foam kinetics and properties of control and CNF/RPUF samples

Sample	V0F-control	V0SF	VCF0.028	VCF0.07	VCF0.14	VCF0.28	V0F- control 2	VCF0.56	VCF0.84	VCF1.12
CNF loading in polyol (% w/w)	0	0	0.028	0.07	0.14	0.028	V0	VC0.56	VC0.84	VC1.12
CNF loading in RPUF[a] (% w/w)	0	0	0.01	0.025	0.05	0.1	0	0.2	0.3	0.4
Part B: polyol blend (by parts)										
Voranol ^{TM} 446	100	100	100	100	100	100	100	100	100	100
Tegostab® B 8460	2.5	2.5	2.5	2.5	2.5	2.5	2.5	2.5	2.5	2.5
Water	1.5	1.5	1.5	1.5	1.5	1.5	1.5	1.5	1.5	1.5
HFCM1	30	30	30	30	30	30	30	30	30	30
DMCHA	1	1	1	1	1	1	1	1	1	1
Part A: pMDI										
NCO index	110	110	110	110	110	110	110	110	110	110
Reaction kinetics										
Mixing time (s)	18	18	18	18	18	18	18	18	18	18
Cream time (s)	28	28	33	45	45	50	28	58	60	59
Gel time (s)	56	58	53	52	70	78	56	100	104	104
Rise time (s)	186	164	135	134	140	144	180	154	154	150
Tack free time (s)	470	392	240	250	310	320	474	420	420	540
Density of cups (kg m^{-3})	41.4	40	44	44	48	47.5	63	62	74	80
Glass transition temperature, T_g (°C) of RPUF	176	177	173	164	165	166	179	176	176	176
Maximum degradation temperature, T_d max (°C) of RPUF	339	350	341	348	336	338	345	336	347	352

[a] Resulting mass fraction.

(Makita HP2071F, stainless steel dissolver shaft with 12 blades) at 2000 rpm for 5 min. The blowing agent (HFCM1) was then added, and the total mixture was blended for a further 5 min. Part A (pMDI) was then added to Part B and mixed at 4000 rpm for 20 s, after which it was immediately poured into a pre-heated mould at 60 °C ($l \times b \times h$: 30 cm × 30 cm × 10 cm) coated with a release agent. Then, the mould was tightly closed using nuts and bolts and allowed to cure for 24 h. The entire mixing was conducted as room-temperature. The weight of pMDI required to achieve a constant 110 isocyanate index was calculated from the experimental hydroxyl values of the polyol blends as described by Pinto et al.[32] The de-moulded RPUF samples were skinned to remove the release agent, and the core of the foam was cut into pieces in accordance with the sample size requirement for each characterisation proposed by Septevani et al.[33]

To understand the influence of CNF on reaction kinetics and flow behaviour during reaction, rheological measurements were performed on resin formulations i.e., without the addition of blowing agents in the foam formulation. The polyurethane resin formulations with CNF (V0R, V0SR, VCR0.028, VCR0.07, VCR0.14, VCR0.28, VCR0.56, VCR0.84, and VCR1.12) were prepared by mixing the CNF/polyol dispersions reported by Haridevan et al.[6] with surfactant and catalyst according to the Part B formulations in Table 1 (and Table S1 in ESI†) without the blowing agents (HFC M1 and water) and then pMDI at a low NCO index of 37 (mixed for 5 s) in order to avoid rapid exothermicity and polymerisation on the rheometer.

2.3. Characterisation

The rheological analysis of the polyurethane resins was carried out using a rheometer (DHR-2 series, TA instruments) at oscillation mode with room temperature (25 °C) and a gap of 500 μm. A disposable parallel plates geometry with a diameter of 25 mm was used for the experiment. Preliminary strain sweeps were conducted at a frequency of 1 Hz to evaluate the linear viscoelastic region. Time sweeps were measured from 10 s (after mixing) to 650 s within the linear viscoelastic region. Excess material from the plates was cleaned before the start of the experiment. The curing kinetics of the CNF/polyurethane resins was measured under dynamic oscillation as a function of time. Although this experimental system has several limitations, including the reduced NCO index and lack of blowing agents, this allowed controlled monitoring in the rheometer and afforded an understanding of the effect of CNF on the reactivity kinetics of CNF/polyol dispersions on reaction with pMDI. No pre-shearing was conducted.

The RPUF samples were characterised by measuring reaction kinetics, density, thermal conductivity and compressive properties. The reactivity of the formulations was measured using a standard cup test (ASTM D7487) to record the cream time, gel time, free rise time, and tack-free time. The apparent core density of the RPUF samples was determined according to ASTM D1622 using a standard specimen of $l \times b \times h$: 51 mm × 51 mm × 40 mm.

Fourier transform infrared spectroscopy (FTIR) was performed on a Thermo-Nicolet 5700 fitted with a diamond attenuated total reflection (ATR) accessory (Thermo Electron Corp., USA). The spectra were further smoothened and normalised. Spectra for RPUF samples were recorded in the wavenumber range of 500–4000 cm^{-1} over 128 scans with a resolution of 4 cm^{-1}. The spectra were further smoothened and normalised. The thermogravimetric analysis was conducted to investigate the thermal properties of the CNF/RPUF using a Mettler Toledo TGA operated by STA-R^e version 9.10 software. The samples were heated in a nitrogen atmosphere using aluminium pans of a standard size of 40 μl. The temperature was initially ramped from room temperature to 40 °C before heating to 480 °C at a constant heating rate of 10 °C min^{-1}. Thermo-mechanical property analysis of the foams was performed on cylindrical specimens (<15 mm diameter) in compression mode on a

dynamic mechanical analyser (DMA) (simultaneous differential thermal analysis (SDTA) 861e, Mettler Toledo GmbH, Switzerland) operated by STA-R^e version 9.10 software. Specimens were tested at a frequency of 1 Hz over a temperature range between $-50\ ^\circ$C and $250\ ^\circ$C with a heating rate of $2\ ^\circ$C min^{-1}.

The surface microstructure of the RPUF was examined using scanning electron microscopy (SEM). RPUF samples were conditioned in liquid nitrogen for 1 min and then fractured and mounted on aluminium stubs for further examination under a tabletop scanning electron microscope (Hitachi TM4000) for microstructural observations. The average cell size (diagonal length) of the RPUF was measured from the SEM images, both parallel and perpendicular to the direction of foam rise, using ImageJ software.

High-resolution microCT imaging of RPUF samples (one specimen for each formulation) were performed using a Skyscan 1272 μCT (version 1.1.19, Bruker, Belgium) desktop X-ray microscopy platform. The scanning parameters were: 50 kV X-ray voltage, 200 μA current, 1300 ms exposure time, no filter, 0.75 μm isotropic voxel size, 0.1° rotation step, 180° scan, 1801 × 1 binning, and 4 frame averaging. The datasets were reconstructed with NRecon (version 1.7.3.1; Bruker, Belgium) and InstaRecon (version 2.0.4.6; University of Illinois, USA) software using cone-beam reconstruction (Feldkamp) algorithm, along with ring artefact reduction and beam hardening corrections.

The tomographs were modified in 2D using CTAn software version 1.16.4 (Bruker, Belgium), and the images were further resized by 4 times. FIJI image processing software (ImageJ, USA) was used to pre-process the CT images to ensure the wall could be reliably distinguished from the space. This was achieved by identifying the wall signal and setting the background information to zero. The images were further processed according to the method optimised by Haridevan *et al.*[34] with the help of IMARIS Surface Wizard which applies water shed algorithm for 3D pore reconstruction. The selected parameters were further quantified.

The thermal conductivity of RPUF was measured using a heat flow meter (FOX200, LaserComp, USA) in the direction parallel to foam rise using three standard samples having dimensions of $l \times b \times h$: 20 cm × 20 cm × 2.5 cm according to ASTM C518-10. The compressive strength and compressive modulus of RPUF were determined using a universal testing machine (Instron 5965) with a 5 kN load cell with six standard samples $l \times b \times h$: 51 mm × 51 mm × 40 mm (per direction to foam rise) in compression mode following standard ASTM D1621-10. The statistical variation between different samples for mechanical properties, thermal conductivity, density, and microstructural parameter measurements, was analysed using an independent *t*-test at a confidence level of 95% ($p < 0.05$) (Tables S2–S11, in ESI†). The error bars represent the standard error of the sample (the standard deviation of the sample population).

3. Results and discussion

3.1. Influence of CNF on the Reactivity of CNF/polyol dispersions

Fig. 1a shows the complex viscosity of the neat resins and the CNF/polyurethane resins as a function of time. The initial

Fig. 1 (a) Complex viscosity of CNF/polyurethane resins dispersions; (b) schematic representation of the effect of CNF on the reactivity of CNF/polyol dispersions at low and high loadings.

increase in complex viscosity ($\sim$10–100 s) of the resins indicates the increased reactivity of CNF/polyol dispersion with pMDI. The neat resins (V0R and V0SR) gradually gained viscosity after $\sim$100 s due to cross-linking with pMDI. However, the rate of increase with V0SR was significantly lower than observed for V0R. At this point in time, the reason for this is unknown, given that there are insignificant differences between the respective control polyols in their spectroscopic and rheological properties.[6] The CNF/polyurethane resins started at higher viscosities than the control resins. Interestingly, resins VCR0.028 and VCR0.07 prepared using CNF/polyol dispersions (VC0.028 and VC0.07) with a viscosity lower than the control polyol,[6] also exhibited higher viscosities than the control resins. Furthermore, both the resins reached their gel time faster than control, despite both having a slower cream time than the control. This shows the enhanced reactivity of these formulations. The onset of complex viscosity increase was faster for the samples with higher CNF loading (red dotted line in Fig. 1a), suggesting the rapid formation of the cross-linked network and reduced mobility of macromolecular chains.

Furthermore, the disturbances caused by shear mixing are not observed for CNF/polyurethane resin, indicating that CNF possibly acts as an effective local "constrainer or confiner" of molecular motion. This is supported by the increase in storage modulus (G') and the reduced differences between loss modulus (G'') and G' (Fig. S1 in the ESI†), which indicates the improvement in the elastic component of the resins as a reinforcement effect of CNF. Given the insignificant changes in OHv of the CNF/polyol dispersions (Table S1 in the ESI†), the increase G' (elastic component) at low CNF loadings is due to

the formation of rigid domains through cross-linking reactions of OH groups with NCO units[35] and secondary (van der Waals and hydrogen bonding) interactions between matrix and CNF.

Resins prepared from dispersion with CNF loading >0.56% w/w exhibited G'–G'' crossovers indicating earlier gelling behaviour[36] within 600 s. These three resins (VCR0.56, VCR0.84, VCR1.12) exhibited a slightly different rheological response, in which the G' gradually increased, after that stabilised with minimal increase in viscosity, possibly due to the network formation with percolated CNF.

The curing kinetics of the CNF/polyurethane resins measured by the rheological response shows that the reactivity of CNF/polyol dispersions with pMDI is predominantly influenced by polyurethane-fibre interactions at low loading, and network formation at high loading fibre–fibre interactions, as schematically illustrated in Fig. 1b. At low loadings, the presence of well-distributed CNF covalently connects with the polymer chains and exhibits increased reactivity of the CNF/polyol dispersion. At high loadings, the presence of percolated CNF networks increases the viscosity, hindering the effective mixing of the CNF/polyol dispersions with pMDI, and thus possibly resulting in minimal/negligible improvement in chemical reactivity. This trend is reflected in the reaction kinetics measured by the standard cup foam test (discussed in the next section).

3.2. Influence of CNF on CNF/RPUF formation

The foaming reaction kinetics of the RPUF samples was examined through a standard cup foam test (Table 1). The gel times of VCF0.028 and VCF0.07 were faster than the control RPUF (V0F and V0SF), and this was attributed to the increased fibre-polymer reactivity at low viscosity CNF/polyol dispersions

(VC0.028 and VC0.07) compared to the neat polyols (V0, V0S) during mixing at high shear rates. In contrast, the reactivity decreased (increased gel time) for the dispersions with the higher CNF loadings, and this was potentially due to the increase in viscosity limiting mixing efficiency and accessibility of the OH groups to pMDI. These observations are in support of the curing kinetics of CNF/polyurethane resins at low NCO index (37), specifically, VCR0.028 and VCR0.07. Furthermore, there was no apparent chemical interaction observed for CNF/RPUF when subjected to ATR-FTIR (Fig. S3 in ESI†).

The thermal stability of CNF/RPUF was characterised using TGA (Fig. S4 in ESI†). As summarised in Table 1, there were slight shifts in maximum degradation temperature (T_d max) for CNF/RPUF but with no significant trend observed. Similarly, the CNF incorporation (incremental loading levels) did not show a significant influence on the storage modulus (G') and $\tan\delta$ obtained from DMA (Fig. S5 in ESI†). In contrast to the significant improvement in G' observed for RPUF nanocomposites with cellulose nanocrystals,[5] only a slight increase in G' for VCF0.07 and VCF0.56 was observed compared to their corresponding control RPUF along with a slight decrease in glass transition temperature (T_g) (Table 1) measured from the $\tan\delta$ peak. This inconsistency improvement in G' and a slight decrease in T_g could indicate the insignificant reinforcement effect of CNF. Despite the improvements observed in rheological responses of CNF/polyurethane resins (i.e. different interactions and two loading regimes), the insignificant reinforcement in RPUF can be attributed to collapsing/coiling nature of CNF during the foaming process (cell formation) and/or low stiffness of CNF. The flexibility and conforming nature of such non-wood-based CNF can be attributed to its

Fig. 2 Scanning electron micrographs of (a) low-density and (b) high-density CNF/RPUF both parallel and perpendicular to foam rise.

high hemicellulose content and residual lignin.[37–39] Also, the influence of CNF was also reflected in the energy dissipation behaviour of CNF/RPUF as a reduction in the magnitudes of tan δ peaks (with broadening).[40]

3.3. Influence of CNF on RPUF microstructure

The influence of different degrees of CNF dispersion in RPUF on the microstructure formation was first investigated using SEM analysis (Fig. 2a and b). The average cell size values (cross-sectional diameter) measured for both low-density and high-density RPUF samples are summarised in Table 2. The control RPUF (V0F) exhibits an average cell size of 663 mm and 669 mm, respectively, for cells measured parallel and perpendicular to the foam rise direction. There is a statistically significant difference between the average cell size of the control RPUF (V0F and V0SF) parallel (−15%) and perpendicular (−21%) to foam rise, and both had a polygonal cell morphology. All the CNF/RPUF nanocomposite samples (Fig. 2a and b) showed a statistically significant decrease in the average cell size compared to V0F with a change in anisotropy. Unlike the control samples (V0F, V0SF and V0F-control 2) which exhibited relatively smaller cell sizes perpendicular to the foam rise than in the parallel direction, the CNF/RPUF nanocomposite samples exhibited smaller average cell sizes in parallel to the foam rise. Specifically, at highest loading level, VCF1.12 showed a statistically significant decrease (−26%) in the average cell size in the direction parallel to rise, but an increase (16%) in perpendicular to foam rise (Table S2 in ESI†).

The decrease in the average cell size observed for low-density CNF/RPUF (VCF0.028, VCF0.07, VCF0.14, VCF0.28) is clearly due to the nucleation effect induced by the well-dispersed CNF in the polyol. However, the decrease in the average cell size for high-density CNF/RPUF (VCF0.56, VCF0.84) is possibly due to combined effect of increased viscosity and nucleation. The nucleation effect inhibits the coalescence of cells during cell formation, resulting in an increased number of smaller cells in the resultant RPUF.[41] With increased loading levels, an increase in viscosity (with nucleation effect) causes reduction in expansion of cells in the foam rise direction during foaming.

Four RPUF samples at different loadings of CNF were examined to investigate the influence of CNF loading on the microstructure of CNF/RPUF using X-ray μCT analysis. Fig. 3a and e shows the 3D reconstructed modelling using the images obtained from X-ray μCT scanning. These models have been used to estimate spatial microstructural parameters, such as cell volume and ellipticity (prolate, oblate and sphericity), and solid skeletal parameters, such as strut volume, strut thickness, strut length, cell wall thickness and cell wall length. The average values of the microstructural parameters (spatial and solid skeletal) are summarised in Table 2, and the statistical significance of the values are summarised in Table S3–S6 in ESI.†

Since the frequency of the values (repetition) is essential for precisely evaluating and correlating the RPUF properties, the distribution of the values is used for further discussion. Furthermore, given the small sample size, the evaluation of

Table 2 The average values of microstructural parameters of CNF/RPUF

Properties	V0F-control	V0SF	VCF0.028	VCF0.07	VCF0.14	VCF0.28	V0F-control 2	VCF0.56	VCF0.84	VCF1.12
Core density (kg m^{-3})	32.7 ± 2.3	31.0 ± 2.4	39.3 ± 3.1	37.9 ± 2.2	39.5 ± 2.0	40.5 ± 4.3	55.6 ± 1.8	53.2 ± 3.5	62.3 ± 2.7	63.1 ± 3.0
SEM analysis										
Average cell size diameter (μm) (∥)	669 ± 59	569 ± 57	308 ± 30	371 ± 15	317 ± 11	362 ± 15	453 ± 24	311 ± 14	314 ± 15	334 ± 17
Average cell size diameter (μm) (⊥)	663 ± 75	522 ± 26	351 ± 21	440 ± 27	355 ± 13	407 ± 19	415 ± 26	345 ± 16	337 ± 18	481 ± 28
Tomographic analysis										
Cell volume (μm^3)	$(6.9 \pm 4.7) \times 10^8$		$(6.3 \pm 1.3) \times 10^7$			$(4.0 \pm 0.3) \times 10^7$				$(4.4 \pm 0.6) \times 10^7$
Oblate ellipticity	0.5 ± 0.1		0.4 ± 0.0			0.4 ± 0.0				0.4 ± 0.0
Prolate ellipticity	0.3 ± 0.0		0.3 ± 0.0			0.3 ± 0.0				0.4 ± 0.0
Cell sphericity	0.5 ± 0.0		0.5 ± 0.0			0.5 ± 0.0				0.5 ± 0.0
Strut volume^a (μm^3)	2.2×10^7		33.2×10^7			3.1×10^7				3.9×10^7
Strut thickness (μm)	18.8 ± 0.3		12.7 ± 0.1			12.8 ± 0.2				11.8 ± 0.2
Strut length (μm)	47.5 ± 0.5		29.3 ± 0.3			30.2 ± 0.3				29.8 ± 0.3
Wall thickness (μm)	3.3 ± 0.0		3.1 ± 0.0			3.1 ± 0.0				3.0 ± 0.0
Wall length (μm)	34.0 ± 0.3		27.4 ± 0.2			25.7 ± 0.2				21.4 ± 0.1
Strut volume fraction^b (fs)	0.9		0.8			0.8				0.8

^{a} Experimentally generated value. ^{b} Calculated from the ratio of strut thickness to the sum of strut and wall thickness.

Fig. 3 (a) Tomographic 3D reconstruction of the skeleton of the scanned CNF/RPUF nanocomposites (view from the top); (b) pore separation highlighted on a representative 2D slice; (c) 3D reconstruction of the scanned CNF/RPUF nanocomposites (view from the side); representative tomographic slices filtered for (d) struts and (e) cell walls. The representative images here have been colour corrected and formatted for better visualisation.

distribution of microstructural parameter values at each loading level is much more relevant than studying the effect of loading level on the average values obtained for each microstructural parameter. However, Fig. S7 and S8 in ESI† show the influence of loading of CNF on the spatial and skeletal microstructural parameters for reference.

3.3.1. Spatial parameters. *Cell volume* is the measure of the space occupied by an individual cell. All CNF/RPUF samples exhibited a statistically significant reduction ($>91\%$) in average cell volume compared to the control RPUF (Fig. 4a, Table 2 and Table S3 in ESI†). Further, the jitter distribution (Fig. 4a) shows that the spread of cell volume in all CNF/RPUF samples was significantly tighter than in the V0F, reflecting the larger number of cells with reduced cell volume due to the increased density of the CNF/RPUF. Nevertheless, large cells (outliers) are still present in both the V0F-control and all CNF/RPUF foams.

Fig. 4b violin chart shows the density plot (width), median (white dot in the centre of the box), interquartile region (length of the inner black box) and range (length of the line that extends out of the black box) of cell sphericity of CNF/RPUF samples and Fig. 4c shows the normalised counts for oblate ellipticity (disk-like shape), prolate ellipticity (cigar-like shape) and sphericity (roundness) of the cells.

A statistically significant reduction (13 to 22%) in the oblate ellipticity was observed for the CNF/RPUF samples with increasing CNF loading up to VCF0.28 (Table 2 and Table S4 in ESI†). This was reflected in the prolate ellipticity and cell sphericity. This shows that the increase of CNF reduces the homogeneity of the cell shape and is clearly observed in the density distribution (width) of the cell sphericity values (Fig. 4b) of VCF0.28. These differences in cell ellipticity at different loadings could be attributed to the differences in alignment and collapse (coiling) of CNF during cell formation and rise.[5] Therefore, it can be summarised that the dispersion and the loading levels of CNF strongly affect the spatial parameters of the RPUF microstructure.

3.3.2. Skeletal parameters. The solid polymer skeleton of the RPUF is constructed of struts (junctions) and walls (faces). The average and distribution values for strut thickness, strut length, wall thickness, wall length, and the average strut volume was estimated from processing the 2D CT tomographs (summarised in Table 2) and the statistical significance of the values are summarised in Tables S5 and S.6 in ESI.†

Fig. 4 Influence of CNF on the (a) cell volume distribution (b) cell sphericity, (c) cell ellipticity (d) strut volume and density of CNF/RPUF. (e) Schematic representation of the effect of fibre distribution (loading level) on the RPUF microstructure.

The average strut thickness and strut length of CNF/RPUF exhibited a statistically significant decrease with the incorporation of CNF (Fig. S6a, b, ESI† and Table 2) compared to the control RPUF (Table S6 in ESI†). The reduced interquartile range and the increased density of the distribution of the values around the median value for CNF/RPUF compared to V0F-control also supports this conclusion. A strong trend was not observed for the variation in strut thickness or strut length, which is attributed to the significant differences in the ellipticity of the cells.

The average cell wall thickness and average wall length of the CNF/RPUF also exhibited a statistically significant decrease with the incremental increase of CNF loading compared to the control RPUF (Fig. S6c, d and Table S5 in ESI†). Statistically significant differences for average wall length were also observed for CNF/RPUF compared to each other (Table S6 in ESI†). The reduction in average wall length suggests the possibility of increased adjacent cells (increased cell coordination number) and/or the total number of cell walls.[42]

As previously discussed, it appears that the CNF, while acting as nanoscale nucleating agents, can align, coil, collapse during the foaming process and affect the formation of cells or cell morphology significantly in many possible ways. Due to the diverse possible morphology of CNF, the spatial microstructural parameters such as cell volume and cell ellipticity (sphericity) are affected. As a consequence of changes in the shape of the cell, the skeletal parameters (strut thickness, strut length, wall thickness, and wall length) simultaneously changes.

The effect of fibre morphology on skeletal parameters is validated by the good correlation ($>70\%$) (Fig. S9 in ESI†) of the average strut volume with the viscosities (at $60\ \text{s}^{-1}$) of the CNF/polyol dispersions (previously reported[6]) and the CNF/polyurethane resins. This correlation indicates that the morphology of struts is influenced by the rheological behaviour of the CNF/polyol dispersions. CNF loading and percolation effects at high loadings are also observed in the struts. Given that the volume of RPUF scanned is constant, the increase in strut volume of CNF/RPUF samples with foam density shows that the struts of CNF/RPUF are heavier than that of V0F-control. This is also supported by the fact that the strut volume is increasing with the relative reduction of strut thickness and wall thickness (Fig. 4c and Table 2). Therefore, it appears that increased solid polymer (represented as strut volume) in CNF/RPUF is redistributed as many thin struts and walls as possible. This concurs well with the inverse correlation of strut volume with average strut thickness and average strut length of CNF/RPUF (Fig. S7 in ESI†). This polymer re-distribution phenomenon was also observed for relatively high lignin load incorporated RPUF.[34]

To summarise, the alignment/collapse/conformation of CNF during the foaming process strongly affects the microstructural formation. The nucleation effect of CNF prompts the formation of a larger number of smaller cells with distinct ellipticity depending on the loading levels and CNF interaction. This subsequently results in differences in the skeletal parameters.

The lack of a significant trend in the changes observed in microstructural parameters with the increase in loading levels was attributed to the two different working mechanisms induced by CNF interaction and dispersion. The schematic representation in Fig. 4e illustrates the effect of CNF/polyol dispersions (fibre–fibre and fibre–polyol interactions discussed in Haridevan et al.[6]) on RPUF at the various loading levels. At low loadings, well-distributed CNF increases the nucleation effect resulting in RPUF with reduced cell volume. As the loading increases, the fibre interaction affects the ellipticity resulting in a more heterogeneous microstructure. Whereas at high loadings, the percolation of CNF bundles results in RPUF with reduced cell volume, not only through nucleation but also due to the high viscosity of the CNF/polyol dispersions and associated constraints foam evolution.

3.4. Influence of CNF on the physical properties of the RPUF

3.4.1. Density. The cup foam densities (Table 1) show that incorporating CNF into RPUF at low loadings up to 0.4% w/w in RPUF can result in a 93% increase compared to the V0F-control. This is also reflected in core densities (Table 3) that

Table 3 Properties of low-density CNF/RPUF samples

Sample	V0F-control	V0SF	VCF0.028	VCF0.07	VCF0.14	VCF0.28	V0F-control 2	VCF0.56	VCF0.84	VCF1.12
Properties										
Core density (kg m^{-3})	32.7 ± 2.3	31.0 ± 2.4	39.3 ± 3.1	37.9 ± 2.2	39.5 ± 2.0	40.5 ± 4.3	55.6 ± 1.8	53.2 ± 3.5	62.3 ± 2.7	63.1 ± 3.0
Compressive strength (MPa) ($\parallel$)	0.2 ± 0.0	0.1 ± 0.0	0.2 ± 0.0	0.2 ± 0.0	0.2 ± 0.0	0.2 ± 0.0	0.4 ± 0.1	0.3 ± 0.0	0.3 ± 0.0	0.3 ± 0.0
Compressive strength (MPa) ($\perp$)	0.1 ± 0.0	0.1 ± 0.0	0.2 ± 0.0	0.2 ± 0.0	0.2 ± 0.0	0.2 ± 0.0	0.4 ± 0.0	0.2 ± 0.0	0.3 ± 0.0	0.3 ± 0.0
Compressive modulus (MPa) ($\parallel$)	3.5 ± 0.3	3.2 ± 0.8	3.9 ± 1.3	4.5 ± 0.9	4.6 ± 1.1	4.7 ± 0.7	8.3 ± 2.4	6.6 ± 0.5	7.2 ± 0.5	6.9 ± 1.7
Compressive modulus (MPa) ($\perp$)	2.8 ± 0.2	3.0 ± 0.6	5.2 ± 0.3	4.5 ± 0.4	4.8 ± 0.2	4.6 ± 0.3	8.3 ± 0.6	5.7 ± 0.3	7.0 ± 0.2	7.4 ± 0.2
Initial λ at RT^a (mW m^{-1} K^{-1})	29.9 ± 2.3	34.7 ± 1.5	24 ± 2.7	28.4 ± 10.6	24.1 ± 3.7	26.9 ± 7.8	30.9 ± 8.0	25.3 ± 1.7	25.6 ± 1.8	25.8 ± 2.1
Aged λ^a (mW m^{-1} K^{-1}): 6 months at RT	32 ± 1.5	36.6 ± 3.3	27.1 ± 4.1	31.4 ± 11.3	26.5 ± 3.2	30.1 ± 11.4	32.8 ± 9.9	27.6 ± 2.3	28.1 ± 2.0	28.3 ± 1.6

^{a} Measured to parallel to rise, λ = thermal conductivity, $\parallel$ = parallel to rise, $\perp$ = perpendicular to rise, and RT = room temperature.

show a statistically significant increase parallel and perpendicular to the foam rise with increased CNF loading. The low viscosity polyol dispersions offered relatively low density RPUF whereas the high viscosity polyol dispersions with percolated networks offered high density RPUF. This strongly indicates that the dispersion and distribution of CNF has a strong impact on the structure of the RPUF, consequentially the density of the foam.

3.4.2. Compressive strength and Young's modulus. The compressive mechanical properties of the neat RPUF and all CNF/RPUF (parallel and perpendicular to foam rise) are summarised in Table 3. The significance and percentage change of the properties compared to V0F-control and V0SF are summarised in Tables S7 and S8 in ESI.† The correlation of specific compressive properties of CNF/RPUF with the microstructural properties of CNF/RPUF has been attempted using heat maps with Pearson correlation (Fig. S9 in ESI†). Given that the correlation of microstructural properties with compressive properties is based on the small piece of the scanned CNF/RPUF sample, the analysis is not expressed in terms of statistical significance but as interpretations with considerable caution.

The comparison of specific compressive properties at various densities is an effective way of evaluating the effect of the CNF on the compressive properties of RPUF. The CNF/RUF with the same relationship between density and compressive property indicate a comparable improvement (Fig. 5). In contrast, the deviation of the values away from the trendline represents significant improvement or decline with respect to the density. All low-density CNF/RPUF, after normalisation by density, exhibited statistically significant improvements in specific compressive strength (18–25%) and specific compressive modulus (35–57%) in comparison to V0F in the direction perpendicular to rise without compromising the properties in the direction parallel to rise.

In comparison to V0SF, VCF0.028 and VC0.07 exhibited significant improvement of 24–27% and 25–39% in specific compressive strength and specific compressive modulus, respectively, in the perpendicular direction to foam rise. This could be attributed to the strong hydrogen bonding of the well-distributed individual CNF in the polyurethane matrix, offering a reinforcement effect[5,9,16] and the potential alignment of CNF in the direction of foam rise allowing effective stress transfer from matrix to filler. Septevani et al.[5] reported that CNC (0.4% w/w) incorporated RPUF exhibited significant improvement specifically in the direction perpendicular to foam rise due to the alignment of CNC in the direction of foam rise.

In contrast, in the high-density CNF/RPUF (Fig. 5), such reinforcement effect was not observed, and the specific compressive properties significantly declined compared to the corresponding high-density control RPUF. This can be attributed to three possible reasons, (i) the heterogenous microstructure of RPUF due to the percolated CNF morphology and high viscosity, (ii) poor stress-transfer between CNF and matrix potentially due to the collapse of CNF bundles in the resultant RPUF and (iii) the CNF from the selected non-wood biomass is
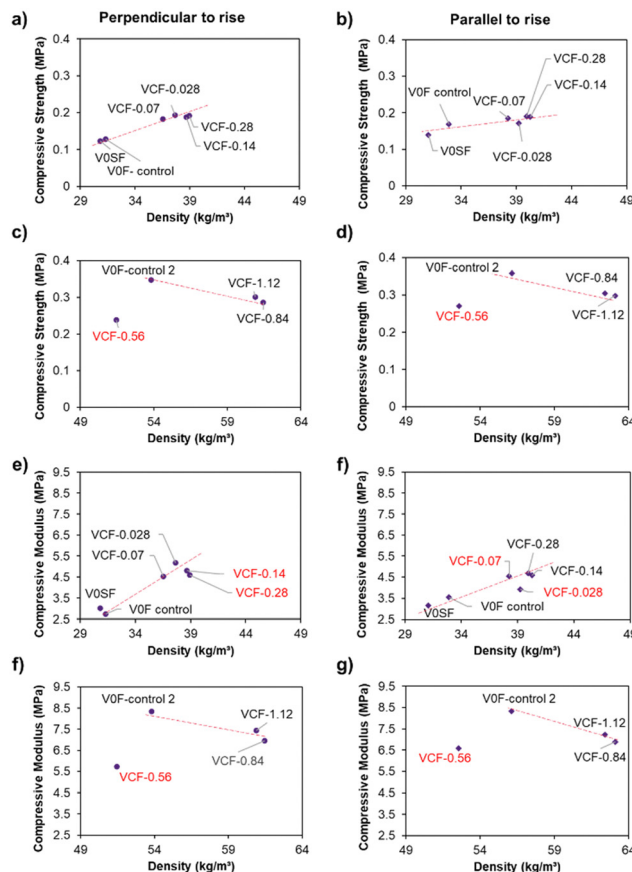

Fig. 5 Specific compressive strength of CNF/RPUF of (a) and (b) low density and (c) and (d) high density and specific compressive modulus of CNF/RPUF of (e) and (f) low density and (f) and (g) high density; both perpendicular and parallel to foam rise (error bars represent standard error and n = 6 samples per direction).

not stiff enough to reinforce foams of high-density. The improved G' observed for CNF/polyurethane resins at high loadings is not reflected for high-density CNF/RPUF, possibly because the relative CNF content is minimal at bulk scale. Hence, it can be postulated that stress transfer occurs well in the low-density CNF/RPUF with low loadings, owing to retained dispersion (from the polyol dispersions) of individual CNF in cell walls.

Overall, the reinforcement effect as reflected in specific compressive properties and the improved reactivity for the low-density CNF/RPUF indicates that the optimal loading of CNF is likely around 0.025% w/w in RPUF. However, this effect is lost for CNF/RPUF above the optimal loading, possibly due to the differences in conformation, alignment, and collapse of the long thin fibres with foam rise, influencing the cell ellipticity and thus decreasing the compressive properties of the resultant RPUF. This is supported by the good correlation of average cell sphericity with the specific compressive properties both parallel and perpendicular to foam rise (Fig. S9 in ESI†). Given the relative lack of significant sampling of measurements of physical properties (n = ~3–12) in comparison to the statically precise microstructural quantification ($\sim n < 400$–$20\,000$),

conclusions were made carefully. Further data collection is required to determine the precise relationships between microstructural and physical properties of the resultant RPUF.

3.4.3. Thermal conductivity of VCF. The effective thermal conductivity of RPUF is strongly influenced by the conductivity and ratio of solid/gas phases and cell parameters (average cell size and the closed-cell content). The influence of changes in microstructure and density of RPUF on the thermal conductivity was investigated. The thermal conductivity of neat RPUF V0SF increases when the polyol is shear processed, reflecting the larger cell size than the control RPUF V0F.

The incorporation of CNF decreased the thermal conductivity of low-density and high-density CNF/RPUF samples (Fig. 6 and Table 3). Given the similar densities and a common blowing agent, VCF0.028 exhibited a statistically significant improvement of 14% and 20% in thermal conductivity, respectively, compared with V0F-control and V0SF predominantly due to the significant reduction in average cell volume (Fig. 4a).

This reduction was observed for the low-density CNF/RPUFs other than VCF0.07 compared to V0SF. This was attributed to the microstructure of RPUF formed from the CNF/polyol

dispersion at rheologically a transient loading level of CNF, as discussed in Haridevan *et al.*[6] VCF0.07 with weak CNF–CNF interactions forming a transient network is observed to strongly influence the cell ellipticity, thus the difference in polymeric pathways, which may increase the effective thermal conductivity.

At higher CNF loading with a similar range of foam density, VCF0.28 exhibits only a 10% statistically significant reduction in effective thermal conductivity despite reduced average cell volume and cell wall thickness and length than VCF0.028. This could be potentially due to the differences observed in the average cell ellipticities of the VCF0.028 (nearly spherical) and VCF0.28 (prolate) (Fig. 6b) manifesting as heterogeneous ellipticity affecting the heat flow.

For high-density CNF/RPUF (Fig. 6b and Table 3), given the similar densities and a common blowing agent with V0F-control 2, a significant reduction in thermal conductivity was observed for VCF0.56. However, further increase in CNF loading did not significantly reduce the thermal conductivity (Table S9 in ESI†), possibly due to the increased strut volume (solid phase) with foam density.

The long-term insulation performance of the RPUF samples was also tested after six months of storage at room temperature (Fig. 6a, b and Table 3). After six months, a statistically significant increase in thermal conductivity was observed for the V0F-control sample.

There was a statistically insignificant difference between thermal conductivity before and after six months for low-density CNF/RPUF, indicating minimal gas diffusion. For the high-density CNF/RPUF, a statistically significant increase in thermal conductivity after six months was observed, indicating the poor retention of gas by the thin cell walls.

Thus, the reduction and the retention of thermal conductivity observed for low-density CNF/RPUF confirm their applicability for thermal insulation in refrigerators and the building industry (BS EN 13165-2012 and BS EN 14315-1:2013) complying with industry specifications in terms of low density (40 kg m^{-3}), compressive strength (>150 kPa), and thermal conductivity (24 mW mK^{-1}).

The long-term insulation performance of the RPUF samples was tested after six months of storage at room temperature (Fig. 6 and Table 3). After six months, a statistically significant increase in thermal conductivity was observed for the V0F-control sample.

There was a statistically insignificant difference between thermal conductivity before and after six months for low-density CNF/RPUF, indicating minimal gas diffusion. For the high-density CNF/RPUF, a statistically significant increase in thermal conductivity after six months was observed, indicating the poor retention of gas by the thin cell walls.

Thus, the reduction and the retention of thermal conductivity observed for low-density CNF/RPUF confirm their applicability for thermal insulation in refrigerators and the building industry (BS EN 13165-2012 and BS EN 14315-1:2013) complying with industry specifications in terms of low density (40 kg m^{-3}), compressive strength (>150 kPa), and thermal conductivity (24 mW mK^{-1}).
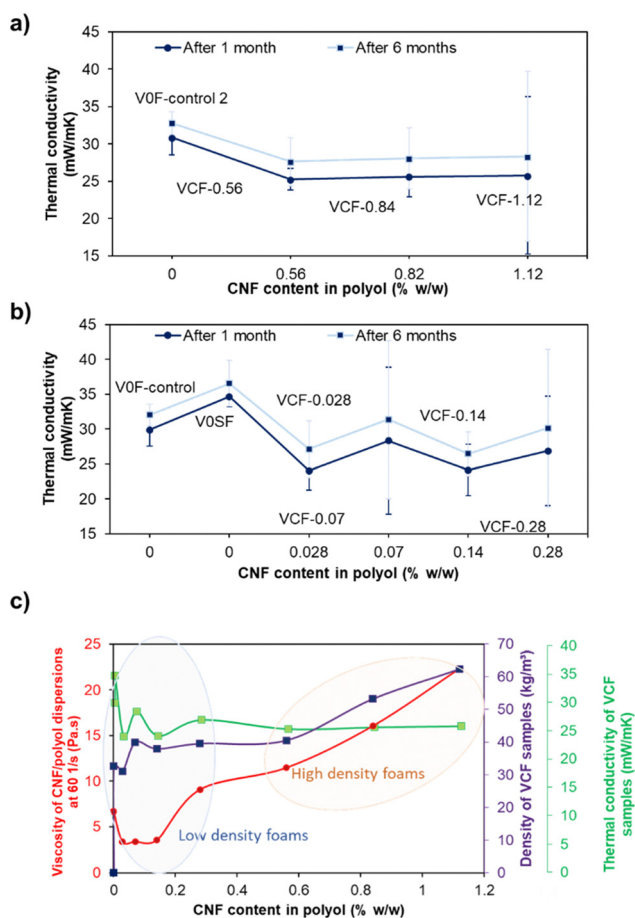
Fig. 6 Initial and aged thermal insulation properties of CNF/RPUF samples ($n = 3$) at (a) low density and (b) high density (c) correlation of viscosity of polyols and density of RPUF samples with the thermal conductivity of respective RPUF samples.

The viscosity of the polyol dispersions showed an interesting association with density and the thermal conductivity of the resultant RPUF samples (Fig. 6c). The low viscosity of the polyol dispersion with the least CNF (0.028% w/w) loading is reflected in the decrease in density and thermal conductivity of the respective sample (0.01% w/w CNF in RPUF) supporting the nucleation effect by nanoparticles reported elsewhere.[4,5,26] CNF/RPUF prepared with 0.07% w/w to 0.028% w/w CNF in polyol exhibited low density; however, the relative inconsistencies observed in the viscosity of the dispersions are reflected in the density and thermal conductivity of the resultant foams. Finally, CNF/RPUF prepared from the percolated polyols (0.056–1.12% w/w CNF in polyol) exhibited high density with an insignificant increase in thermal conductivity. These trends show that the rheological behaviour of the polyols (controlled by loading level, morphology, dispersion and distribution of CNF) has a substantial impact on the microstructure and physical properties of the resultant RPUF.

4. Conclusions

This study demonstrates the preparation of RPUF containing between 0.01% w/w to 0.4% w/w CNF using the CNF/polyol dispersions prepared through the water-assisted dispersion method. It was observed that CNF/polyol dispersions with low CNF loadings, up to 0.2% in polyol, afforded a low-density RPUF (30–50 kg m^{-3}), whereas the CNF/polyol dispersions with higher loadings, 0.56% to 1.12% w/w in polyol, resulted in RPUF with high-density (50–80 kg m^{-3}).

The structural characterisation of CNF/RPUF indicated that the incorporation of CNF generates microstructural changes over chemical changes. 2D cross-sectional analysis and 3D reconstruction analysis shows that the dispersion of CNF in the polyol is retained in the microstructure of the RPUF. On the evaluation of the microstructural parameters, it was observed that the self-interaction of CNF (fibre–fibre interaction) in the polyol and its loading level in RPUF distinctly affected the microstructural parameters of the CNF/RPUF. CNF/polyol dispersions with low loadings promoted nucleation, reducing the average cell size of RPUF. In contrast, the CNF/polyol dispersions with higher loadings appear to influence the microstructure formation through both the increase in viscosity and nucleation effects. This shows that the broad range of rheological properties of these CNF/polyol dispersions can be exploited for controlling or engineering microstructure and consequently tailor the physical properties of foam.

Author contributions

The manuscript was written through contributions of all authors. All authors have given approval to the final version of the manuscript.

Conflicts of interest

There are no conflicts to declare.

Acknowledgements

References

1 Dow Plastics, *Technical information of Voranol™ 446*, The Dow Chemical Company, USA, 2001.

2 T. Widya and C. W. Macosko, *J. Macromol. Sci., Part B: Phys.*, 2005, **44**, 897–908.

3 X. Cao, L. J. Lee, T. Widya and C. Macosko, *Polymer*, 2005, **46**, 775–783.

4 H. Haridevan, M. S. McLaggan, D. A. C. Evans, D. J. Martin, T. Seaby, Z. Zhang and P. K. Annamalai, *ACS Appl. Polym. Mater.*, 2021, **3**, 3528–3537.

5 A. A. Septevani, D. A. C. Evans, P. K. Annamalai and D. J. Martin, *Ind. Crops Prod.*, 2017, **107**, 114–121.

6 H. Haridevan, C. Chaleat, L. Pooley, D. A. C. Evans, P. J. Halley, D. J. Martin and P. K. Annamalai, *Polymer*, 2022, **255**, 125130.

7 G. Harikrishnan, S. N. Singh, E. Kiesel and C. W. Macosko, *Polymer*, 2010, **51**, 3349–3353.

8 M. Kirpluks, A. Ivdre, A. Fridrihsone and U. Cabulis, *Polimery*, 2020, **65**, 719–727.

9 X. Zhou, J. Sethi, S. Geng, L. Berglund, N. Frisk, Y. Aitomäki, M. M. Sain and K. Oksman, *Mater. Des.*, 2016, **110**, 526–531.

10 H. Haridevan, D. A. C. Evans, D. J. Martin and P. K. Annamalai, *Ind. Crops Prod.*, 2022, **185**, 115129.

11 Y. Li and A. J. Ragauskas, *RSC Adv.*, 2012, **2**, 3347–3351.

12 R. J. Moon, A. Martini, J. Nairn, J. Simonsen and J. Youngblood, *Chem. Soc. Rev.*, 2011, **4**, 3941–3994.

13 Y. C. Ching, M. Ershad Ali, L. C. Abdullah, K. W. Choo, Y. C. Kuan, S. J. Julaihi, C. H. Chuah and N.-S. Liou, *Cellulose*, 2016, **23**, 1011–1030.

14 G. Siqueira, J. Bras and A. Dufresne, *Polymers*, 2010, **2**, 728–765.

15 Y. Li, H. Ren and A. J. Ragauskas, *Nano-Micro Lett.*, 2010, **2**, 89–94.

16 J. Andersons, M. Kirpluks and U. Cabulis, *Materials*, 2020, **13**, 2725.

17 H. Fan, A. Tekeei, G. J. Suppes and F.-H. Hsieh, *J. Appl. Polym. Sci.*, 2013, **127**, 1623–1629.

18 W. Leng, J. Li and Z. Cai, *Polymers*, 2017, **9**, 597.

19 W. Leng and B. Pan, *Forests*, 2019, **10**, 200.

20 A. A. Septevani, D. A. C. Evans, D. J. Martin and P. K. Annamalai, *Ind. Crops Prod.*, 2018, **112**, 378–388.

21 O. Faruk, M. Sain, R. Farnood, Y. Pan and H. Xiao, *J. Polym. Environ.*, 2013, **22**, 279–288.

22 M.-C. Li, Q. Wu, R. J. Moon, M. A. Hubbe and M. J. Bortner, *Adv. Mater.*, 2021, 2006052.

23 O. Nechyporchuk, M. N. Belgacem and F. Pignon, *Biomacromolecules*, 2016, **17**, 2311–2320.

24 X. J. Zhou, M. M. Sain and K. Oksman, *Composites, Part A*, 2016, **83**, 56–62.

25 A. I. Cordero, J. I. Amalvy, E. Fortunati, J. M. Kenny and L. M. Chiacchiarelli, *Carbohydr. Polym.*, 2015, **134**, 110–118.

26 A. A. Septevani, D. A. C. Evans, D. J. Martin, P. Song and P. K. Annamalai, *Polym. Compos.*, 2023, **44**(12), 8857–8869.

27 D. Yan, L. Xu, C. Chen, J. Tang, X. Ji and Z. Li, *Polym. Int.*, 2012, **61**, 1107–1114.

28 X. Cao, L. James Lee, T. Widya and C. Macosko, *Polymer*, 2005, **46**, 775–783.

29 M. Zhu, S. Bandyopadhyay-Ghosh, M. Khazabi, H. Cai, C. Correa and M. Sain, *J. Appl. Polym. Sci.*, 2012, **124**, 4702–4710.

30 A. Lorenzetti, M. Roso, A. Bruschetta, C. Boaretti and M. Modesti, *Polym. Adv. Technol.*, 2016, **27**, 303–307.

31 K. Oksman, Y. Aitomäki, A. P. Mathew, G. Siqueira, Q. Zhou, S. Butylina, S. Tanpichai, X. Zhou and S. Hooshmand, *Composites, Part A*, 2016, **83**, 2–18.

32 M. L. Pinto, *J. Chem. Educ.*, 2010, **87**, 212–215.

33 A. A. Septevani, PhD thesis, The University of Queensland, 2016.

34 H. Haridevan, D. Barkauskas, K. A. Sokolowski, D. A. C. Evans, D. J. Martin and P. K. Annamalai, *ACS Appl. Polym. Mater.*, 2023, **5**, 6772–6780.

35 A. A. Septevani, D. A. C. Evans, C. Chaleat, D. J. Martin and P. K. Annamalai, *Ind. Crops Prod.*, 2015, **66**, 16–26.

36 V. M. Wik, M. I. Aranguren and M. A. Mosiewicki, *Polym. Eng. Sci.*, 2011, **51**, 1389–1396.

37 J. Pennells, I. D. Godwin, N. Amiralian and D. J. Martin, *Cellulose*, 2020, **27**, 575–593.

38 K. Kępa, C. M. Chaléat, N. Amiralian, W. Batchelor, L. Grøndahl and D. J. Martin, *Cellulose*, 2019, **26**, 6555–6569.

39 A. Hosseinmardi, P. K. Annamalai, B. Martine, J. Pennells, D. J. Martin and N. Amiralian, *ACS Omega*, 2018, **3**, 15933–15942.

40 X. Xu, F. Liu, L. Jiang, J. Y. Zhu, D. Haagenson and D. P. Wiesenborn, *ACS Appl. Mater. Interfaces*, 2013, **5**, 2999–3009.

41 L. R. Glicksman, J. Stewart, N. Solomou and A. Cunningham, *Thermal Envelopes VI/Insulation-Princlples*, 1988, **VI**, 25–32.

42 S. Pardo-Alonso, E. Solórzano, L. Brabant, P. Vanderniepen, M. Dierick, L. Van Hoorebeke and M. A. Rodríguez-Pérez, *Eur. Polym. J.*, 2013, **49**, 999–1006.